1-1-1999

Effects of Secondary Electron Emission on Charge Pulses from a Z-Stack Microchnnel Plate Photon Counting Detector with a Crossed Delay Line Anode Readout

Alan W. Bird
Utah State University

EFFECTS OF SECONDARY ELECTRON EMISSION ON CHARGE PULSES FROM A Z-STACK MICROCHANNEL PLATE PHOTON COUNTING DETECTOR WITH A CROSSED DELAY LINE ANODE READOUT

Alan W. Bird

Los Alamos National Laboratory
Space and Remote Sensing Sciences Group, MS D436, Los Alamos, NM 87545

Abstract

A study of the effects of secondary electron emission on charge pulses from a microchannel plate (MCPs) photon counting detector with crossed delay line (CDL) anode readout is presented. The detector is a two-dimensional photon counting detector with fast count rate and good spatial resolution being developed at Los Alamos National Laboratory. The CDL anode is constructed of two orthogonal planar pairs of helically wound wires on inner and outer ceramic sides attached to a copper ground plane. The electron cloud event from the MCPs interacts with the wires generating a signal pulse. The electrons that strike the wire with sufficient energy generate secondary electrons. A model is presented for the charge pulses from the CDL anode incorporating the effects of secondary electron emission. An empirical test of the model is conducted with two different wire materials using a demountable MCP/CDL detector. Charge pulses are measured and the results are compared to the model. The results show that the charge pulses from the CDL anode are material dependent and exhibit the general behavior predicted by the model. Secondary electron emission is an integral part of the CDL anode charge pulses and must be considered in further developments of the CDL anode readout.

Keywords: Crossed delay line anode, microchannel plates, secondary electron emission, position sensitive detector

1. INTRODUCTION

The microchannel plate/crossed delay line (MCP/CDL) detector is a two-dimensional photon counting detector with fast count rate, 1×10^6 count/sec, and good spatial resolution, <30μm, being developed at Los Alamos National Laboratory.[1] The MCP/CDL detector employs microchannel plate (MCP) photon counting technologies with CDL anode readout. The CDL anode (figure 1) is constructed of two orthogonal planar pairs of helically wound wires on inner and outer ceramic sides attached to a copper ground plane. An electron cloud event from the MCPs is accelerated into the anode striking each of the four wires and the ground plane. Each wire collects a portion of the electron cloud event. The electron cloud event generates a signal on the delay line that propagates in both directions to the ends of the line. The delay lines are read out at both ends of each axis resulting in four charge pulses. The position of the event is determined by timing difference of the signal at each end of the delay lines. In the process secondary electrons (SEs) are generated.

The demountable MCP/CDL detector consists of a vacuum chamber with a quartz entrance window, light baffles, z-stack of MCPs, and CDL anode. A z-stack of MCPs is used for an electron gain of $\approx10^7$ electrons.[2-4] The demountable MCP/CDL detector is operated at approximately 1×10^{-7} torr vacuum. The system is setup such that the CDL anode can be exchanged without changing the MCPs orientation.

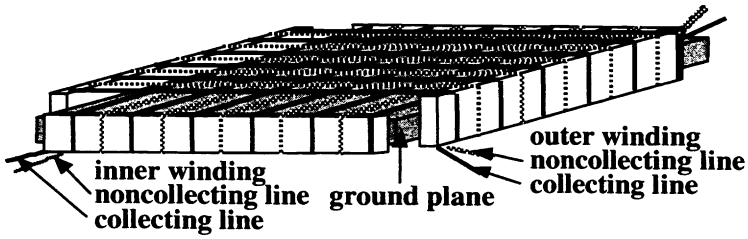

Figure 1: Crossed delay line anode.

The CDL anode (figure 1) is made of a copper ground plane with pairs of outer ceramic sides, 9.53mm height, and inner ceramic sides, 6.35mm height, attached. Evenly spaced wire pairs are wound in a double helix on the inner and outer ceramics sides giving orthogonal inner and outer windings that are separated by 1.59mm. The wire pairs are distinguished by designating one wire of a winding pair as the collecting line (c) and the other wire as the noncollecting line (nc).

The detector is operated by applying separate voltages to input and output of the MCPs, outer collecting line, outer noncollecting line, inner collecting line, inner noncollecting line, and ground plane. The bias between the MCPs is set to operate the MCPs at a specific electron gain while adjusting the voltage at the output of the MCPs to obtain the desired accelerating potential, V_a. Each of the four wires and the ground plane can be held at separate potentials. These potentials can be adjusted to manipulate the collection of the electron cloud event and distribution of the SEs. The potentials are adjusted until the optimum signal condition is achieved.

The semiempirical theory of secondary electron emission has been introduced in previous work.[5-8] A set of empirical equations developed by Vaughan to fit experimental data and to provide a more precise formula for use in computer models of secondary electron emission is given.[9]

A model is presented for the charge pulses from the MCP/CDL detector incorporating the effects of secondary electron emission. Important parameters of the model are describe and investigated. The geometrical relation between the MCPs electron cloud event and the CDL anode wires is described. A two part experimental test of the model is conducted with copper and platinum wire materials using a demountable MCP/CDL detector setup.

The first test in this work examines the overall behavior of the CDL anode and tests for conservation of charge between the CDL anode and the MCPs. This test is only conducted with the platinum wire material. The results are analyzed on the basis of the model and secondary electron emission. The results of this test give an overall understanding of how the electron cloud event and SEs are distributed to the various CDL anode components.

The second test in this work is a test of the model. The model is developed for the charge pulse from one wire of the CDL anode setup to remove all SEs. This experiment measures the charge pulse from that wire using CDL anodes constructed with copper and platinum wire materials. The results are presented and then compared to the model. These results show that the charge pulses from the CDL anode are material dependent and have the general behavior predicted by the model. Differences between the experimental results and the predicted results are discussed based on secondary electron emission, the knowledge of the electron cloud event from the MCPs, and the charge collection of the CDL anode.

This study was conducted to understand the effect of secondary electron emission on charge pulses from the MCP/CDL detector. To develop a model for the charge pulses from the MCP/CDL detector and to experimentally test that model. Secondary electron emission plays a crucial role in the operation of position sensing anodes used in imaging MCP intensifiers.[10]

2. SECONDARY ELECTRON EMISSION

Austin and Stark (1902) first discovered secondary electron emission.[11] They observed that a metal bombarded by energetic electrons had a larger number of electrons emitted from the surface than were incident upon it. Salow (1940) and Bruning (1954) developed the semiempirical theory of secondary electron emission.[5, 6] Vaughan (1989) developed an empirical set of equations that provides one of the best fit to experimental data and incorporates the angle of incidence.[9, 12]

Primary electrons (PEs) are the electrons incident onto a material with energy E_{PE}. Two groups categorize the energy distribution of electrons leaving the surface of a material bombarded by energetic PEs.[6-8] The first group is defined as true secondary

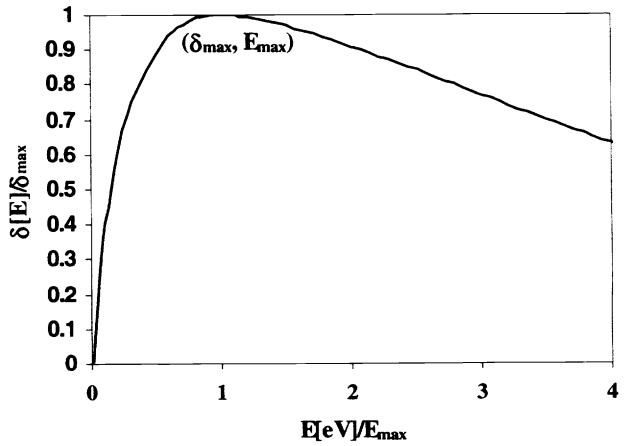

Figure 2: Universal curve of secondary electron emission.

electrons (SEs) and is comprised of electrons with energies up to 50eV. The second group is elastically and inelastically reflected PEs with energies up to the PEs impact energy. Interposed on the energy distribution are Auger electron peaks.

The secondary electron emission coefficient δ is defined as the number of true SEs emitted per PE. It has been observed that the δ coefficient is a function of the energy of the electrons incident onto a material, the angle of incidence, and the material.[6-8] The δ coefficient for all materials exhibiting secondary electron emission follows a universal curve (figure 2) that increases to δ_{max} at PE energy E_{PEmax} then decreases as PE energy continues to increase.

2.1 Semiempirical theory of secondary electron emission

Dionne (1975) reviews the elementary semiempirical theory of secondary electron emission and Seiler (1983) gives an indepth review of secondary electron emission.[13, 8]

From the semiempirical theory of secondary electron emission a reduced yield expression is arrived at

$$\delta(E_r)/\delta_{max} = 1.11E_r^{-0.35}\left(1-e^{-2.3E_r^{1.35}}\right), \tag{1}$$

where $E_r=E_{PE}/E_{PEmax}$. This reduced yield equation provides a fit to the universal curve data.[14]

The derivations for the semiempirical theory of secondary electron emission assume that the PEs are incident normal to the surface and penetrate straight into the material. It is found empirically that δ increases as a function of incident angle.[6-8]

2.2 A new formula for secondary electron emission

Vaughan developed a set of empirical equations that provide one of the best fit to experimental data and incorporate the angle of incidence, the set of equations have been confirmed to fit well to experimental data.[9,12] The equations are fit to data obtained with monoenergetic PEs for a defined angle of incidence.

According to Vaughan the reduced yield equation is given by

$$\delta/\delta_{max} = \left(ve^{1-v}\right)^k, \tag{2}$$

$$v = E_i - E_0/E_{max} - E_0 \tag{3}$$

The energy where δ_{max} is reached is E_{max}. The minimum energy needed to generate SEs is E_0, which is taken as 12.5V.[9] The impact energy of PEs is E_i and k is an empirical fit parameter, $k=k_1=0.62$ for $v<1$ and $k=k2=0.25$ for $v>1$. If a smooth variation of k is desired then k is given by

$$k = \frac{k_1+k_2}{2} - \frac{k_1-k_2}{\pi}\arctan(\pi \ln v). \tag{4}$$

If the PEs impact at an angle θ(rad), as measured from the normal, then the empirical correction equation for E_{max} is given by

$$E_{max}(\theta) = E_{max}(0)\left(1+\frac{k_{SE}\theta^2}{2\pi}\right) \tag{5}$$

and the empirical correction equation for δ_{max} is given by

$$\delta_{max}(\theta) = \delta_{max}(0)\left(1+\frac{k_{S\delta}\theta^2}{2\pi}\right), \tag{6}$$

where k_{SE} and $k_{S\delta}$ are smoothness fit factors that depend on the surface of the material. When the smoothness of the material is unknown then $k_{SE}=1$ and $k_{S\delta}=1$ are used. These formulas, as in the semiempirical theory, require that one know the values for δ_{max} and E_{max}. The values of δ_{max} and E_{max}, for many materials, can be found in the literature of secondary electron emission.[8, 15]

3. MODEL FOR SECONDARY ELECTRON EMISSION AND THE CROSSED DELAY LINE CHARGE PULSES

A UV photon strikes the MCPs generating an electron cloud event of $\approx 1\times10^7$ electrons (Q_t). The electron cloud event is accelerated onto the CDL anode by the potential difference between the MCPs and the anode, V_a, striking the CDL anode wires and ground plane with some energy, E_a, generating SEs at all four wires and ground plane. A CDL anode biasing scheme is setup to remove generated SEs from the outer noncollecting line. The outer collecting line, inner collecting line, inner noncollecting line, and ground plane are held at a higher potential than the outer noncollecting line. Some fraction of the electron cloud event ($-Q_{nc}$) strikes the outer noncollecting line generating SEs. The SEs are removed from the outer noncollecting line giving rise to a positive charge pulse ($+Q_{SE}$) on the outer noncollecting line. The charge pulse measured on the outer noncollecting line is the sum of theses two charge pulses and is given by

$$Q_S = Q_{SE} - Q_{nc}. \tag{7}$$

The δ coefficient can be written as

$$\delta = Q_{SE}/Q_{nc}. \tag{8}$$

Solving for Q_{SE} in equation (8) and substituting it into equation (7) an expression for the charge pulse from the outer noncollecting line is arrived at,

$$Q_S = Q_{nc}(\delta - 1). \tag{9}$$

There are two parts to the expression for the charge pulse from the noncollecting line that need to be understood. First, the fraction of the electron cloud event that strikes the outer noncollecting line, Q_{nc}. The fraction of the electron cloud event that strikes the noncollecting line depends on the behavior of the electron cloud event from the MCPs, the electron cloud event's geometry to the CDL anode, and the electric field of the CDL anode. Second are the secondary electron effects. The δ coefficient in equation (9) is for a cylindrical wire bombarded with PEs that have an energy distribution. The δ coefficient for monoenergetic primary electrons and a defined angle of incidence is well understood and equation (2) can be used to compare known behavior of secondary electron emission to the measured charge pulses from a cylindrical wire.

3.1 Electron cloud event and the crossed delay line

It is well known that the electron cloud event from MCPs follow a quasi-Gaussian pulse height distribution that is characterized by the peak to valley ratio (PVR) and the pulse height resolution (PHR).[16] Eberhardt gives a description of the MCPs parameters and the electron cloud event's behavior as it transits between the MCPs and the anode.[17] Assuming that the electron cloud event originates from one pore of the MCPs it will strike the anode with diameter W_a given by

$$W_a = 3.3L_a(v_{mt}/V_a)^{1/2}, \tag{10}$$

where v_{mt} is the mean tangential energy of an electron from the MCPs and L_a is the distance from output of the MCPs to the anode (figure 3).

As the accelerating potential V_a increases the electron cloud event diameter W_a decreases. Considering the geometrical relationship between the electron cloud event diameter W_a and the CDL anode wires one can arrive at an understanding of how Q_{nc} varies as a function of V_a.

A program was written to demonstrate the geometrical relation between the electron cloud event and the outer noncollecting line. The outer wire plane can be described as a plane with evenly distributed bars of width D equal to the diameter of a wire. Superimposed on the plane is an electron cloud event disk of diameter W_a. Define A_{nc} as the ratio of the charge pulse Q_{nc} to the total electron cloud event charge Q_t. A geometrical description of A_{nc} is arrived at by calculating the ratio of the areas of noncollecting line within the electron cloud event diameter W_a to the area of W_a. The following four assumptions were used to calculate A_{nc}: 1) The total electron cloud event charge Q_t is contained within a disk of diameter W_a. 2) The electron cloud event electrons are homogeneously distributed within W_a. 3) The electron cloud event strikes the wire plane perpendicularly. 4) The wires are evenly distributed.

The program calculated A_{nc} for the electron cloud event striking the CDL anode over the following three conditions: 1) The electron cloud event centered on collecting line. 2) The electron cloud event centered on noncollecting line. 3) The electron cloud event centered between collecting line and noncollecting line. The program then calculated the average of these three

conditions giving a weight of two to the third condition. Results from the program were obtained with the parameters 25eV<Ea<1500eV, vmt=1eV, La=10mm, and D=0.14mm (figure 4).

The results of this program clearly show that there is a geometrical relationship yet the results are inconclusive. For simplicity, the charge that strikes the noncollecting line will be taken as a constant for electron cloud events that strike the CDL anode over all conditions of centering. The electric fields of the CDL anode will also have an effect on the charge collection. The sum of all these effects may or may not have a significant effect on the charge collection and will be left to a further study.

3.2 Secondary electron emission and crossed delay line wires

The values for δ_{max} and E_{max} are available for monoenergetic PEs incident normal to the material surface.[8, 15] For the CDL anode the PEs have an energy distribution and are incident upon cylindrical wires. Assuming that the electron cloud event is homogeneously distributed and strikes the wires perpendicular to the wire plane then the PEs strike the wires over all angles of incidence from $-\pi/2$ to $+\pi/2$. An estimate of the average $<\delta_{max}>$and $<E_{max}>$ are found by using an integral average of equation (5) and equation (6) with k_{SE} and $k_{S\delta}$ equal to one. The averages for $<E_{max}>$ equations (5) is,

$$< E_{max} >= \frac{1}{\pi} \int_{-\frac{\pi}{2}}^{+\frac{\pi}{2}} E_{max}(0) \left(1 + \frac{\theta^2}{2\pi} \right) d\theta = 1.13 E_{max}(0), \tag{11}$$

and $<\delta_{max}>$ equation (6) is,

$$< \delta_{max} >= \frac{1}{\pi} \int_{-\frac{\pi}{2}}^{+\frac{\pi}{2}} \delta_{max}(0) \left(1 + \frac{\theta^2}{2\pi} \right) d\theta = 1.13 \delta_{max}(0). \tag{12}$$

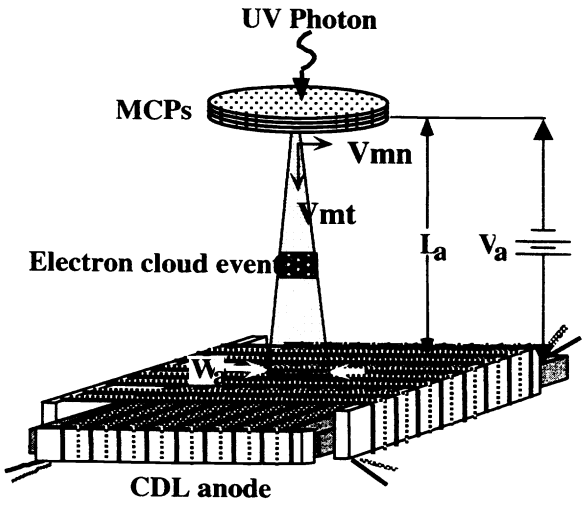

Figure 3: Electron cloud event footprint on the CDL. The diameter of the footprint is W_a, the accelerating potential from the MCPs to the anode is V_a, the mean tangential energy of an electron from the MCPs is v_{mt}, and the distance from output of the MCPs to the anode is L_a.

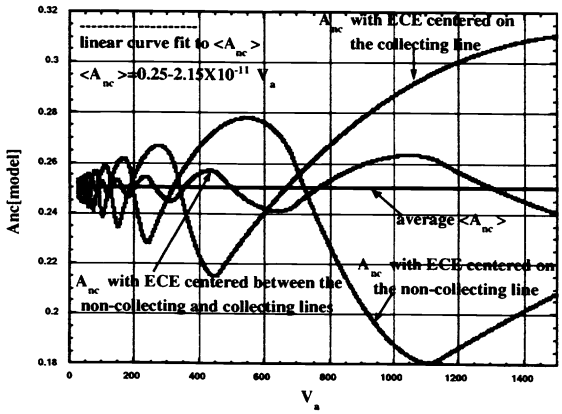

Figure 4: Plot of A_{nc} for the electron cloud event centered on collecting line, the electron cloud event centered on noncollecting line, the electron cloud event centered between collecting line and noncollecting line, and the average. The values used to calculate A_{nc} were 25eV<E_a<1500eV, v_{mt}=1eV, L_a=10mm, and D=0.14mm.

3.3 Predictions from the model

The charge pulse from the noncollecting line will be material dependent and will follow the general behavior given by equation (9). The pulse height distribution of charge Q_{nc} will follow the quasi-Gaussian behavior characteristic of MCPs.

In practice the MCPs are illuminated by UV light over a finite area generating electron cloud events that strike the CDL anode wires over all conditions of electron cloud event centering. For simplicity and based on the geometrical analysis (figure 4) the fraction of electron cloud event that strikes the noncollecting line is taken as the average and is assumed to be constant.

Two wire materials, copper (Cu) and platinum (Pt), were used to test the model. The values $E[eV]_{max}$=500-600 and δ_{max}=1.10-1.30 for Cu are taken from Seiler[8] with average values $<E[e]_{max}>$=565-678 and $<\delta_{max}>$=1.24-1.47 calculated with equations (11) and (12), respectively. The values $E[eV]_{max}$=700-750 and δ_{max}=1.35-1.70 for Pt are taken from Seiler[8] with average values $<E[e]_{max}>$=792-848 and $<\delta_{max}>$=1.53-1.92 calculated with equations (11) and (12), respectively. The reduced yield for the charge pulse from a wire material bombarded by PEs biased to remove SEs is given by

$$Q_{RY} = \frac{Q_S}{Q_{nc}(<\delta_{max}>-1)} = \frac{(\delta-1)}{(<\delta_{max}>-1)}. \quad (13)$$

This equation can be used to compare know behavior of secondary electron emission to the measured charge pulses from the noncollecting line biased to remove generated SEs. The reduced yields for a flattened wire bombarded with monoenergetic PEs biased to remove generated SEs are plotted for Cu and Pt (figure 5) using equation (2) in equation (13) with the larger calculated average values of $<\delta_{max}>$ and $<E_{max}>$.

The charge pulse from the outer noncollecting line, biased to remove SEs, will be negative until it reaches a point where secondary electron emission is unity at which point it will go positive. The positive charge pulse will continue to increase until it reaches $<\delta_{max}>$ at PE energy $<E_{max}>$. Then it will decrease as PE energy increases.

4. MEASUREMENT SETUP, RESULTS, AND ANALYSIS

4.1 Setup for measurements of the outer noncollecting line charge pulses

The z-stack was assembled with three 40mm Galileo MCPs with length to diameter ratio of 40:1, 10μm pore diameter, 12.5μm center-to-center spacing, and 8° bias angle. An Oriel Hg(Ar) lamp (254nm) UV source was used to illuminate the MCPs with a ≈5mm diameter spot.

A constant MCP operating bias was maintained while varying the voltage at the input and output of the MCPs to set the electron cloud accelerating potential, V_a. The CDL anode was held at a constant voltage with the ground plane (g) at 60V, outer collecting line (c) at 35V, inner collecting line (in) at 35V, inner noncollecting line (in) at 35V, and outer noncollecting line (nc) at 5V. The charge pulses were measured from the outer noncollecting line with an AMPTEK A250 charge sensitive preamplifier and read out by a multichannel analyzer system.

The accelerating potential was taken as

$$E_a(eV) = 35eV - (-HiV_2). \quad (14)$$

The 35eV is from 5eV to account for the potential of the noncollecting line and a 30eV mean energy from the MCPs.[18] The voltage at the output of the MCPs is -HiV_2.

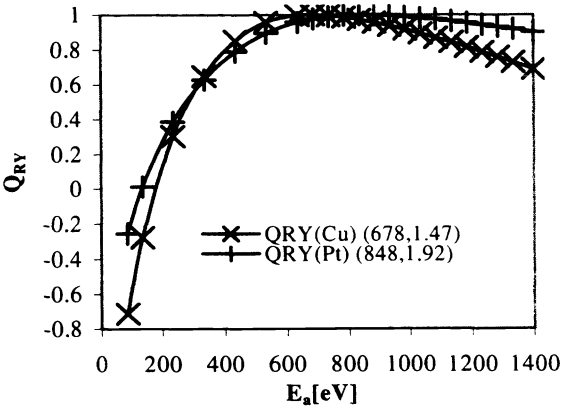

Figure 5: The reduced yields for a flattened wire bombarded with monoenergetic PEs setup to remove generated SEs are plotted for Cu and Pt using equation (2) in equation (13) with the larger calculated average values for Copper $<E[e]_{max}>$=678 and $<\delta_{max}>$=1.47 and for Platinum with $<E[e]_{max}>$=848 and $<\delta_{max}>$=1.92.

Two anodes were tested. The first anode was built with 0.14mm-diameter bare Zirconium-Copper (CuZr) alloy (Cu-0.14%Zr) wire. The second anode was built with 0.13mm-diameter bare Rhodium-Platinum (PtRh) alloy (Pt-6%Rh) wire.

4.2 Charge collection of the electron cloud event and distribution of generated secondary electrons

A slight modification to the setup for measuring the charge pulses from the outer noncollecting line was introduced to gain a better understanding of the charge distribution of the electron cloud event and distribution of generated secondary electrons to the CDL anode components. This experiment also tested for conservation of charge between the MCPs and the CDL anode. The behavior of all five components of the CDL anode and the MCPs was studied by measuring the equivalent current with the same CDL anode and MCP biasing scheme used to measure the charge pulses from the noncollecting line.

The equivalent current of the MCPs electron cloud event was measured independently from the five equivalent currents of the CDL anode components. To check for conservation of charge the equivalent current of the MCPs electron cloud event was compared to the sum of the five equivalent currents of the CDL anode components. This was accomplished by isolating the MCPs and their power supplies with an isolation transformer creating a closed system that loses charge via the electron cloud event (figure 6). The charge loses from the MCPs closed system is collected by the five CDL anode components. The MCPs electron cloud event equivalent current was determined by measuring the voltage drop across a high precision resistor connected between the power supplies ground and the anode ground.

The inner windings four wire ends were connected to give a single inner plane collecting component (in). The outer collecting line (c) two wire ends were connected, the outer noncollecting line (nc) two wire ends were connected, and the ground plane (g) two wire ends were connected. The equivalent currents of the outer collecting line, outer noncollecting line, inner plane, and ground plane were measured separately while the other three were taken to the CDL anode ground. Three equivalent current data sets were obtained using the PtRh winding with a MCPs operating bias of –3700V and four different values for E_a. The average equivalent currents of these three data sets were plotted with y-axis error bar of the standard deviation and x-axis error bars of +/- 20eV due to the uncertainty in the electron's initial energies (figure 7).

Analysis of figure 6 with the effects of secondary electron emission considered can help explain the results of these current measurements. The analysis also gives a better understanding of the collection of the electron cloud event and the distribution of the generated SEs. Secondary electrons are generated at all of the components of the CDL anode. The biasing scheme determines how SEs are distributed, collected, and/or reabsorbed. Some fraction of the SEs will be reabsorbed depending on the CDL anode electric fields. The equivalent currents measured on each component are based on the collection of the electron cloud event, the generated SEs which are removed or reabsorbed, and the distribution of the generated SEs which are removed. The measured currents are given by Iim (i=c,nc,in,g) and the fractions of the electron cloud event that strikes each of the CDL anode components are given by Ii (i=c,nc,in,g).

The secondary electron emission coefficient δ_1 represents the SEs generated at the noncollecting line, δ_2 represents the SEs generated at the inner collecting lines, and δ_3 represents the SEs generated at the outer collecting line. The secondary electron emission coefficient δ_4 represents the SEs generated at the outer collecting line from the SEs generated at the outer noncollecting line accelerated through a 30V gap. The secondary electron emission coefficient δ_5 represents the SEs generated at the inner collecting lines from the SEs generated at the outer noncollecting line accelerated through a 30V gap. The factor β represents the fraction of the SEs generated at the noncollecting lines that are distributed throughout the CDL anode components. Inherent in β is the complex electric field structure and the geometry of the CDL anode.

This analysis must be kept in perspective. The β factors here have imbedded in them reflected primary electrons and the efficiency of removing the generated SEs. The efficiency of removing SEs before they are reabsorbed depends on the electric fields of the detector and the geometry of the CDL anode.

Referring to figure 6 it is seen that the current on the outer noncollecting line and the inner collecting lines can be negative or positive depending on the amount of SEs generated. The current on the outer collecting line and the ground plane will always be negative. The sum of all four currents is the equivalent current of the electron cloud event from the MCPs.

The geometry of the CDL anode can be used to estimate what fraction of the electron cloud event that strikes each CDL anode component. It is reasonable to believe that the fraction of the total electron cloud event that strikes the outer collecting and noncollecting lines is 25% or greater. The remaining 50% of the electron cloud goes through to the inner winding collecting

and noncollecting lines with their fraction being 25% or greater of the remaining 50% each, 12.5%. The remaining 25% or less of the electron cloud event going through to the ground plane. These fraction are represented by the following equalities,

$$I_c/I_t = I_{nc}/I_t = I_{in}/I_t = I_{in}/I_t = 25\%, \tag{15}$$

where I_t is the measured total current. From figure 6 there are four equations and eight unknowns, indeterminate.

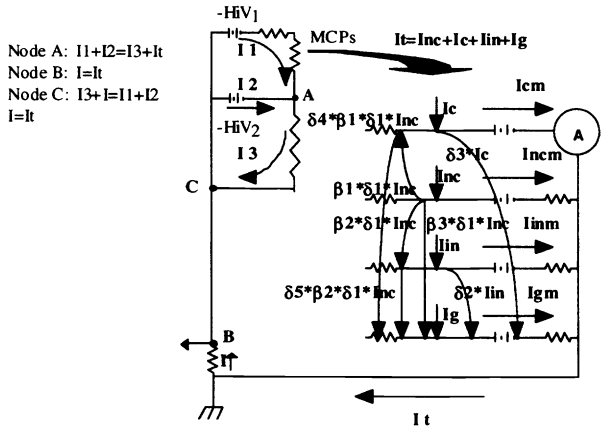

The measured currents (m)
Icm=Ic+δ4*β1*δ1*Inc-δ3*Ic-δ4*β1*δ1*Inc
Incm=Inc-δ1*Inc β1+β2+β3=1
Iinm=Iin+β2*δ1*Inc-δ2*Iin-δ5*β2*δ1*Inc
Igm=Ig+β3*δ1*Inc+δ2*Iin+δ5*β2*δ1*Inc+δ3*Ic+δ4*β1*δ1*Inc

Figure 6: Schematic of the collection of the electron cloud event and distribution of the generated secondary electrons. The equations represent the measured currents incorporating the generated secondary electrons and the condition that the generated secondary electrons on the noncollecting line are conserved. Equivalent circuit and nodal analysis for measurements of the charge collection of the electron cloud event and distribution of generated secondary electrons.

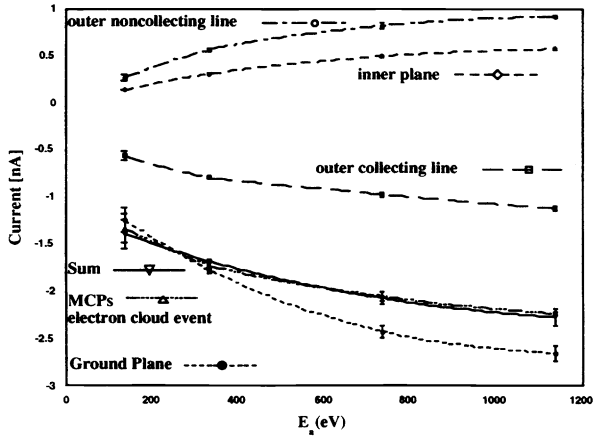

Figure 7: Average equivalent currents using the PtRh winding with a MCPs operating bias of –3700V and four different values for E_a. The y-axis error bars are the standard deviation and x-axis error bars are +/- 20eV due to the uncertainty in the electron's initial energies.

Based on the experimental setup we can solve the second equation of figure 6 for the secondary electron emission coefficient δ_1,

$$\delta_1 = 1 - I_{ncm}/I_{nc}. \tag{16}$$

The calculated values for δ_1 using the equivalent current data and the geometrical values for the distribution of the electron cloud event was plotted along with the second equation using the δ_{max} and E_{max} values found from equation (16) (figure 8).

The δ_1 coefficient from the equivalent current measurements has a larger δ_{max} and E_{max} than predicted in the model, $<\delta_{max}>=2.64$ from measurements compared to $<\delta_{max}>=1.92$ from the model and $<E[e]_{max}>=1150$eV from measurements compared to $<E[e]_{max}>=848$eV from the model. At the lower energies the measured δ_1 curve deviates from the empirical fit equation (2). This deviation is also observed in the measurements of the next test. This comparison between equation (2) and the measured values from the CDL anode are based on secondary electron emission with two different sets of conditions. Equation (2) is valid for monoenergetic electrons with a defined angle of incidence. To make a valid comparison to equation (2) the reflected electrons must also be considered. These measurements can not account for the scattered electron effect on the measured δ coefficient. Yet, the measured values here are consistent with expectations based on secondary electron emission with some deviations from equation (2) due to the measurement system.

The charge was determined by dividing the average equivalent current by the average count rate and is plotted with y-axis error bar of the standard deviation and x-axis error bars of +/- 20eV due to the uncertainty in the electron's initial energies (figure 9). A count rate dependence on Va was observed yet unsubstantiated. These values only serve to give an estimate of the total charge from the MCPs, $Q_{tm} \approx 2.4 \times 10^7$ electrons.

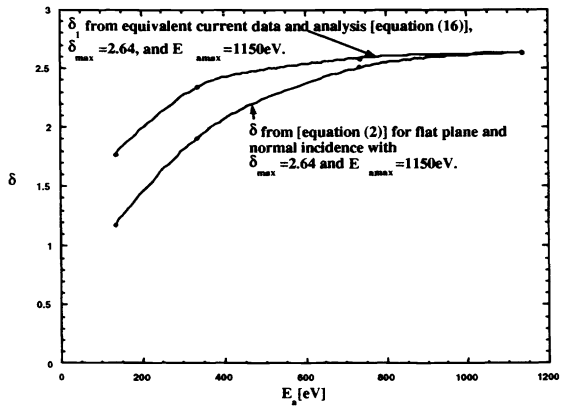

Figure 8: The calculated values for δ_1 using equation (16), the equivalent current data, and the geometrical values for the distribution of the electron cloud event are plotted along with equation (2) using the values found from δ_1.

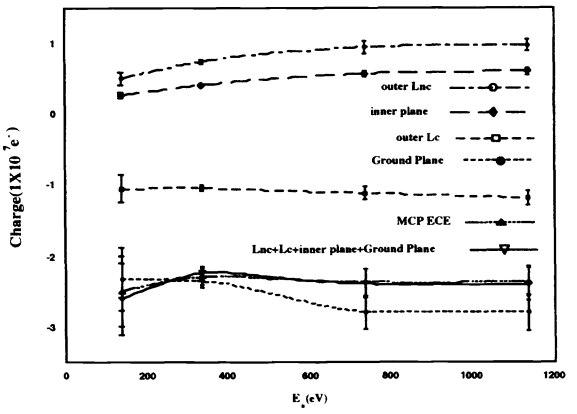

Figure 9: Charge collections determined by dividing the average current by the average count rate. The y-axis error bars are the standard deviation and x-axis error bars are +/- 20eV due to the uncertainty in the electron's initial energies.

These measurements were a limited data set intended only to support the following noncollecting line charge pulse measurements. These measurements suggest a more fundamental approach at modeling and explaining the charge pulses from the MCP/CDL detector. These results are consistent with the behavior expected from secondary electron emission. It is evident from figures 7 and 9 that the charge collected by the CDL anode is consistent with the charge leaving the MCPs. There is no unknown contribution to the charge being collected by the CDL anode.

4.3 Results of the outer noncollecting line charge pulse measurements

Charge pulses from the outer noncollecting line, $Q_s(E_a)$, were measured with the setup described earlier in section (4.1). The charge pulses from both of the windings had a standard MCP quasi-Gaussian pulse height distribution with a PHR of approximately 100%. The count rate was set to minimize pile up. Charge pulse height distributions from the outer noncollecting line, $Q_s(E_a)$, were measured for the CuZr winding with MCPs operating at –3900V (figure 10). The CuZr winding was replaced by the PtRh winding and $Q_s(E_a)$ was measured with MCPs operating at –3900V and MCPs operating at –3700V. The value of MCPs operating at –3700V was used to reach 1400eV energies. The results for the PtRh winding with MCPs operating at –3900V are plotted with the results for the CuZr winding with the MCPs operating at –3900V (figure 11). The results for the PtRh winding with MCPs operating at –3700V are plotted (figure 12).

The reduced yields for CuZr and PtRh windings were calculated by dividing all data points in a set by the maximum charge reached at E_{amax}. The determination of E_{amax} was accomplished by fitting a parabola to the top three data points of each set. The average energy maximums and standard deviations from the averages for the CuZr winding are $\langle E_{amax} \rangle = 850 \pm 38$eV and for the PtRh winding are $\langle E_{amax} \rangle = 1143 \pm 53$eV. The averages for CuZr and PtRh were plotted with error bars of the standard deviation from the average for the y-axis and with error bars of ±20eV for the x-axis (figure 13).

4.4 Analysis

The charge pulses from the outer noncollecting line are material dependent. The charge pulses from both of the windings had a standard MCP quasi-Gaussian pulse height distribution with a PHR of approximately 100%. The general behavior of the measured reduced yields is similar to the behavior predicted from the model.

Measurement of charge pulses at the lowest accelerating potential, 50V, were all positive charge pulses. There was no evidence of negative charge pulses from the noncollecting line as predicted from the model. From the equivalent current measurements on the PtRh winding a larger $<\delta_{max}>=2.64$ was calculated and the overall behavior of the measured secondary electron emission curve deviated from the secondary electron emission curve based on equation (2). The measured reduced yield for CuZr was plotted with equation (13) using equation (2) with $<\delta_{max}>=2.0$, arbitrarily picked to be larger than the predicted value, and $<E_{amax}>=850$ (figure 14). The measured reduced yield for PtRh was plotted with equation (13) using equation (2) with $<\delta_{max}>=2.64$, from the equivalent current measurements, and $<E_{amax}>=1143$ (figure 15).

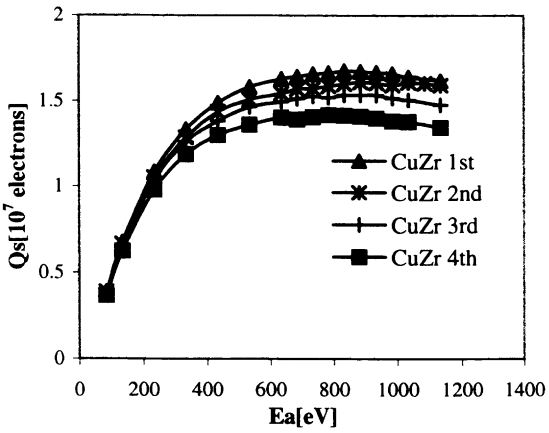

Figure 10: Plot of Qs data sets 1st through 4th for CuZr CDL winding. Data sets were taken in chronological order of 1st through 4th. V_{MCPout} was adjusted while holding ΔV_{MCP} at -3900V. The count rate was changed between the second and third data sets.

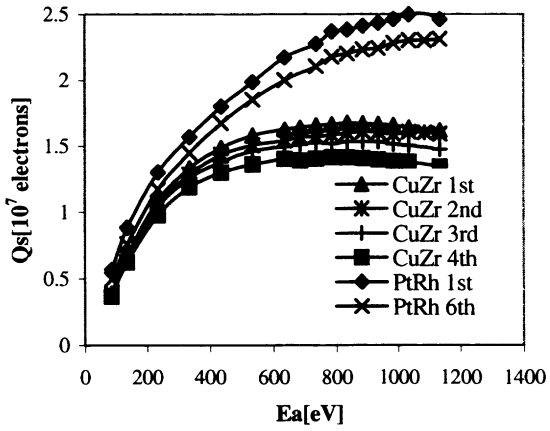

Figure 11: Plot of Qs data sets 1st through 4th for the CuZr CDL winding with Qs data sets 1st and 6th for the PtRh CDL winding. Data sets were taken in chronological order of 1st CuZr through 6th PtRh. V_{MCPout} was adjusted while holding ΔV_{MCP} at -3900V. The UV light source and the count rate were changed between the 1st and 6th PtRh measurements.

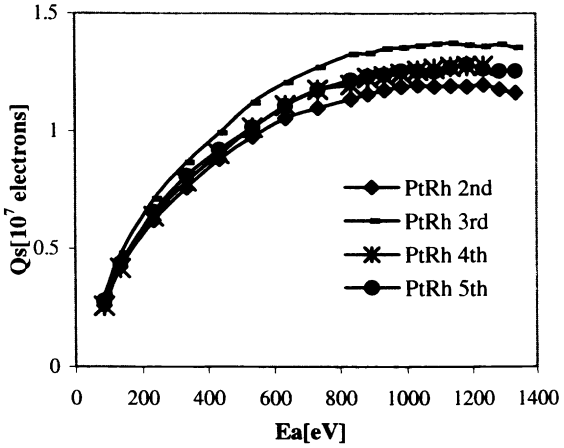

Figure 12: Plot of Qs data sets 2nd through 5th for the PtRh CDL winding. Data sets were taken in chronological order of 2nd through 5th. V_{MCPout} was adjusted while holding ΔV_{MCP} at -3700V. The UV light source and the count rate were changed between the 2nd and 3rd PtRh measurements.

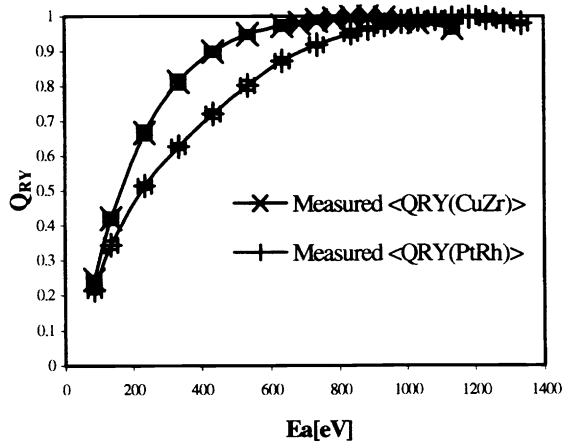

Figure 13: Plot of average reduced yields for CuZr and PtRh CDL windings. The y-axis error bars are the standard deviation of the average reduced yield data and the x-axis error bars are given ±20eV due to the uncertainty in the electron's initial energies.

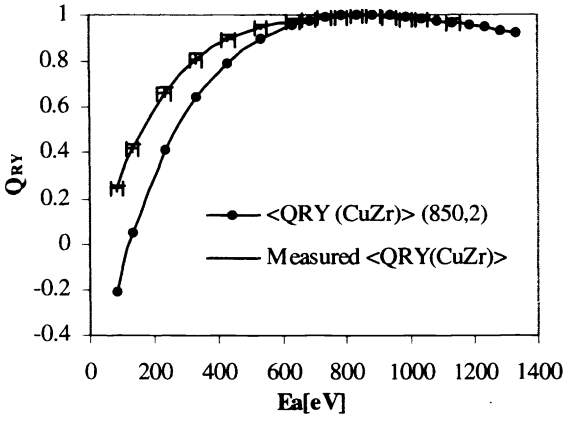

Figure 14: The measured reduced yield for CuZr was plotted with calculated values from equation (13) using equation (2) with $<\delta_{max}>=2.0$, arbitrarily picked to be larger than the predicted value, and $<E_{amax}>=850$. The value for $<E_{amax}>$ was determined by fitting a parabola to the top three data points of each set then finding the average and standard deviation, $<E_{amax}>=850\pm38$eV.

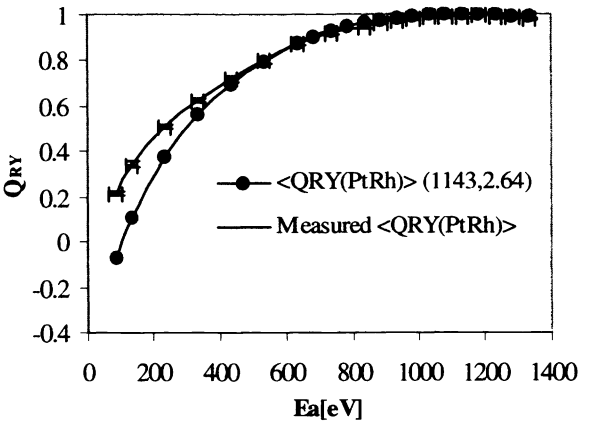

Figure 15: The measured reduced yield for PtRh was plotted with calculated values from equation (13) using equation (2) with $<\delta_{max}>=2.64$, from the equivalent current measurements, and $<E_{amax}>=1143$. The value for $<E_{amax}>$ was determined by fitting a parabola to the top three data points of each set then finding the average and standard deviation, $<E_{amax}>=1143\pm53$eV.

The $<\delta_{max}>$ values being higher, the $<E_{amax}>$ values being higher, and the deviation of the two curves are likely due to the angular dependence of secondary electron emission and the scattered electrons. The energy distribution of the electrons from the MCPs may also contribute to this behavior. There is also a material difference that has not been accounted for, CuZr and PtRh. It is uncertain if these differences are due to secondary electron emission of the cylindrical wire, the geometry of the CDL anode components, the complex electric fields of the detector, or the energy distribution of the electron cloud event. It is likely a combination of all these factors.

5. CONCLUSION

The experimental results presented here clearly show that the charge pulses from the CDL anode are material dependent, follow a general secondary electron emission curve, and have the characteristic quasi-Gaussian pulse height distribution expected from MCPs. These general behaviors were predicted from the model. The premises of the model are simple, yet the CDL anode is complex in its geometry and electrical field structure which complicates the model considerable.

These results give us a better understanding of the charge pulses from the MCP/CDL detector and a better understanding of the physics of the charge collection process of the CDL anode. The results will help in further design and operation of the CDL anode readout.

REFERENCES

1. M.H. Baron and W.C. Priedhorsky, "Crossed delay line detector for ground and space based applications," *Proc. Soc. Photo-Opt. Instrum. Eng. 2006*, pp. 188-197, 1993.
2. J. Cortez and B Laprade, "Long life microchannel plate (L2MCP)," *Proc. Soc. Photo-Opt. Instrum. Eng. 427*, pp. 53-57, 1983.
3. B.N. Laprade and R.J. Labich, "Microchannel plate-based detectors in mass spectrometry," *Spectroscopy 9 (5)*, pp. 26-30 1994.
4. "MCP assembly," Technical Note, Hamamatsu Photonics K.K (1991).

5. H. Salow, "On secondary electron yield of electron bombarded insulators," *Z. Tech. Phys. 21*, pp. 8, 1940.
6. H. Bruning, *Physics and Applications of Secondary Electron Emission*, McGraw-Hill Book Co., Inc., New York, 1954.
7. A.J. Dekker, *Solid State Physics*, Prentice-Hall, Inc., 1957.
8. H. Seiler, "Secondary electron emission in the scanning electron microscope," *J. Appl. Phys. 54 (11)*, pp. R1-R18, 1983.
9. J. Rodney M. Vaughan, "A new formula for secondary electron emission," *IEEE Trans. Electron Devices 36 (9)*, pp. 1963-1967, 1989; "Secondary emission formulas," *IEEE Trans. Electron Devices 40 (4)*, pp. 830, 1993.
10. J.S. Lapington, "The effects of secondary electron emission on the operation of position sensitive anodes," *Nucl. Instrum. and Meth. In Phys. Res. A 392*, pp. 336-340, 1997.
11. L. Austin und H. Starke, "Über die Reflexion der Kathodenstrahlem und eine damit verbudene neue Erscheinung sekundärer Emission," *Ann. Phys. Lpz. 9*, pp. 271, 1902.
12. A. Shih and C. Hor, "Secondary emission properties as a function of the electron incidence angle," *IEEE Trans. Nucl. Sci. 40 (4)*, pp. 824-829, 1993.
13. Gerald F. Dionne, "Origin of secondary-electron-emission yield-curve parameters," *J. Appl. Phys. 46 (8)*, pp. 3347-3351, 1975; "Effects of secondary electron scattering on secondary emission yield curves," *J. Appl. Phys. 44 (12)*, pp. 5361-5364, 1973.
14. R.E.Simon and B.F.Williams, "Secondary-electron emission," *IEEE Trans. Nucl. Sci. 15*, pp. 167-170, 1968.
15. Robert C. Weast, Melvin J. Astle, and William H. Beyer, *CRC Handbook of Chemistry and Physics 68th EDITION 1987-1988*, editors, pp. E-366, CRC Press, Inc. Florida, 1987.
16. K. Oba, C. Okuyama, and H. Kume, "Characteristics and applications of microchannel plates," *Technical Note, Hamamatsu Photonics K.K.*.
17. E. H. Eberhardt, "Parameters pertaining to microchannel plates and microchannel plate devices," *Technical Note No. 127, ITT Electro-optical Products Division*, August 1980.
18. Wiza JL, "Microchannel plate detectors," *Nucl. Instrum. Methods 162(#1-3)*, pp. 587-601, 1979.